Available online at www.sciencedirect.com
ScienceDirect
Journal of Power Sources 162 (2006) 1099–1103
JOURNAL OF POWER SOURCES
www.elsevier.com/locate/jpowsour

Short communication

Development of ruthenium-based bimetallic electrocatalysts for oxygen reduction reaction

Lingyun Liu, Jong-Won Lee, Branko N. Popov *

Center for Electrochemical Engineering, Department of Chemical Engineering, University of South Carolina, Columbia, SC 29208, USA

Received 14 July 2006; accepted 1 August 2006
Available online 12 September 2006

Abstract

Ruthenium-based bimetallic electrocatalysts with non-noble metals such as Ti, Cr, Fe, Co and Pb were synthesized on a porous carbon support using a chelation process. Rotating ring disk electrode measurements indicated that $RuFeN_x/C$ showed the catalytic activity and selectivity toward the four-electron reduction of oxygen to water comparable to those of the conventional Pt/C catalysts. The performance of the membrane-electrode assembly prepared with the $RuFeN_x/C$ cathode catalyst was evaluated for 150 h of continuous operation.

Keywords: Ruthenium; Bimetallic electrocatalyst; Oxygen reduction; Proton exchange membrane fuel cell

1. Introduction

The low activity of cathode catalysts toward oxygen reduction reaction (ORR) which involves multiple electron transfer steps is one of the major impediments to the commercialization of proton exchange membrane (PEM) fuel cells. Even on pure platinum, the most active oxygen reduction material, potentials in excess of 300 mV are lost from the thermodynamic potential for ORR due to competing water activation reaction and sluggish kinetics [1]. Also, Pt remains an expensive metal of low abundance, and it is thus of great interest to find Pt-free metal alternatives used for PEM fuel cells.

Ru-based chalcogenides of chevrel-phase type (e.g. $Mo_4Ru_2Se_8$) were synthesized from a solid-state reaction of pure elements at high temperatures between 1200 and 1700 °C. They showed the significant catalytic activity and selectivity toward the four-electron reduction of O_2 to H_2O in acidic media [2]. The octahedral mixed metal clusters of Ru and Mo in chevrel-phase serve as the electron reservoirs which facilitate electron transfer from the catalyst particle to the adsorbed O_2, thereby increasing the catalytic activity [3]. Recently, low temperature methodologies have been developed to prepare amorphous chalcogenides (e.g. $Mo_xRu_ySe_z$ and Ru_xSe_y) by using metal carbonyls [4]. Ru/carbide/carbonyl complexes formed on the nano-scale Ru colloids are believed to be the catalytically active sites for ORR. Selenium was suggested that acts as a bridge to transfer electrons between the Ru-complexes and the colloids [5].

In our previous work [6] a novel process was developed to synthesize the carbon-supported Ru chelate (RuN_x/C) electrocatalysts for ORR. $RuCl_3$ and propylene diammine as the Ru- and N-precursors were used to synthesize the catalyst. Rotating ring disk electrode (RRDE) experiments indicated that the optimized RuN_x/C catalyst exhibited an onset potential for ORR as high as 0.9 V(NHE) which is comparable to that of the conventional Pt/C catalyst. The catalyst generated less than 2% hydrogen peroxide (H_2O_2) during ORR.

The objective of this study is to synthesize Ru-based bimetallic catalysts using a chelation approach. The bimetallic catalysts were prepared which contain different non-noble alloying metals such as Ti, Cr, Fe, Co and Pb, and their catalytic activities toward ORR were screened using RRDE in an acidic medium. The most promising catalyst ($RuFeN_x/C$) was subjected to extensive materials and electrochemical characterization studies including the performance test of membrane-electrode assembly (MEA).

* Corresponding author. Tel.: +1 803 777 7314; fax: +1 803 777 8265.
E-mail address: popov@engr.sc.edu (B.N. Popov).

0378-7753/$ – see front matter © 2006 Elsevier B.V. All rights reserved.
doi:10.1016/j.jpowsour.2006.08.003

2. Experimental

2.1. Catalyst preparation

The desired amounts of $RuCl_3 \cdot xH_2O$ and $Me(NO_3)_y \cdot zH_2O$ (Me = Ti, Cr, Fe, Co and Pb) were dissolved in isopropyl alcohol (100 mL). The solution was refluxed at 80–90 °C under stirring conditions. Next, propylene diammine was added into the solution to form Ru–Me–N complexes, followed by the addition of carbon black powders (0.4 g of Ketjen Black). The resulting powder specimens were heat-treated in an argon atmosphere at 800 °C for 1 h. The atomic Ru:Me ratio in the catalyst was kept at 1:1, and the amount of catalyst loaded on the carbon support was 20 wt.%.

2.2. Physical characterizations

In order to identify the crystal structures of the synthesized catalysts, X-ray diffraction (XRD) patterns were recorded with an automated Rigaku diffractometer using Cu Kα radiation over the scanning angle range of 10–70° at the scan rate of 4° min^{-1}. To determine the particle size of the catalyst, transmission electron microscopy (TEM) was performed using a Hitachi H-8000 at 200 keV.

2.3. Rotating ring disk electrode measurements

The RRDE experiments were performed in a three-electrode electrochemical cell using a bi-potentiostat (Pine Instruments) at room temperature. An RRDE with gold ring (5.52 mm inner-diameter and 7.16 mm outer-diameter) and glassy carbon disk (5.0 mm diameter) was used as the working electrode. The catalyst ink was prepared by blending the catalyst powder (8 mg) with isopropyl alcohol (1 mL) in an ultrasonic bath. The catalyst ink (15 μL) was deposited onto the glassy carbon disk which was previously polished with Al_2O_3 powder. After drying, 10 μL of a mixture of Nafion solution (5 wt.%) and isopropyl alcohol was coated onto the catalyst layer to ensure better adhesion of the catalyst on the glassy carbon substrate. The electrolyte was 0.5 M H_2SO_4 solution. A platinum mesh and an $Hg/HgSO_4$ electrode were used as the counter and reference electrodes, respectively. All potentials in this work were referred to a normal hydrogen electrode (NHE).

In order to estimate the double layer capacitance, the electrolyte was deaerated by bubbling with N_2, and the cyclic voltammogram was recorded by scanning the disk potential between 0.04 and 1.04 V(NHE) at a rate of 5 mV s^{-1}. Then, the electrocatalytic activity for ORR was evaluated in the oxygen-saturated electrolyte. The oxygen reduction current was taken as the difference between currents measured in the deaerated and oxygen-saturated electrolytes. The ring potential was held at 1.2 V(NHE) to oxidize H_2O_2 generated during ORR.

2.4. Performance test of membrane-electrode assemblies

The cathode catalyst ink was prepared by ultrasonically blending catalyst powder (0.2 g) with Nafion solution (5 wt.%) and isopropyl alcohol for 5 h. The catalyst ink was sprayed onto the gas diffusion layer (GDL) (ELAT LT 1400 W, E-TEK). The process was repeated until a total loading of supported catalyst of 6 mg cm^{-2} was achieved. A commercially available catalyzed GDL (20 wt.% Pt/C, 0.4 mg cm^{-2} Pt, E-TEK) was used as the anode for all fuel cell tests. A thin layer of Nafion (0.4 mg cm^{-2}) was coated on both the anode and cathode surfaces to improve the adhesion between the catalyst layer and the membrane. The Nafion-coated anode and cathode were hot-pressed to the Nafion 112 membrane at 140 °C and at 50 atm for 90 s. The geometric area of the MEA used was 5 cm^2.

The MEA tests were carried out in a single cell with serpentine flow channels. Pure hydrogen gas humidified at 77 °C and pure oxygen humidified at 75 °C were supplied to the anode and cathode compartments, respectively. Polarization technique was conducted with a fully automated test station (Fuel Cell Technologies Inc.) at 75 °C and at ambient pressure.

3. Results and discussion

3.1. Catalytic activities of various Ru-based bimetallic catalysts

Fig. 1 shows polarization curves on the rotating disk electrodes for Ru-based bimetallic catalysts with different non-noble alloying metals. As shown in Fig. 1, the onset potential for ORR strongly depends on the alloying metal in the bimetallic catalyst. The $RuFeN_x/C$ catalyst exhibits the onset potential for ORR as high as 0.9 V(NHE) and the well-defined limiting current below 0.5 V(NHE).

The Koutecky–Levich equation was used to calculate the kinetically limited current I_k [7]:

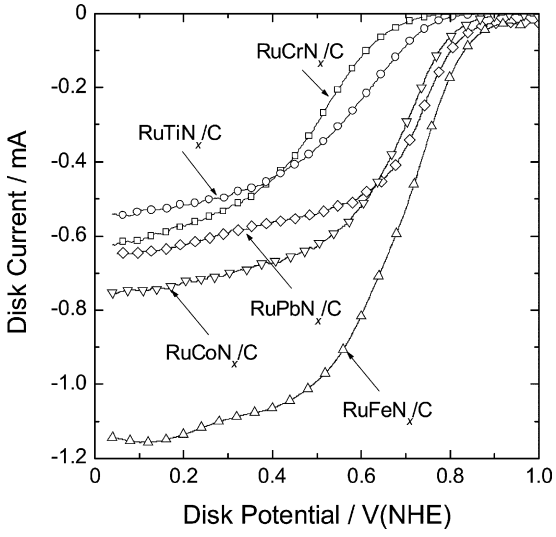

Fig. 1. Polarization curves on the rotating disk electrodes for different Ru-based bimetallic catalysts: $RuTiN_x/C$, $RuCrN_x/C$, $RuFeN_x/C$, $RuCoN_x/C$ and $RuPbN_x/C$. The measurements were performed in 0.5 M H_2SO_4 solution saturated with oxygen at the potential scan rate of 5 mV s^{-1} and the rotation speed of 900 rpm.

$$\frac{1}{I_d} = \frac{1}{I_k} + \frac{1}{I_l} + \frac{1}{I_f} = \frac{1}{nFAkC_{O_2}} + \frac{1}{0.2nFAD_{O_2}^{2/3}\omega^{1/2}\upsilon^{-1/6}C_{O_2}} + \frac{L}{nFAC_fD_f} \quad (1)$$

where I_d is the measured disk current, I_l the diffusion limited current, I_f the Nafion film diffusion limited current, n the number of electrons exchanged in the electrochemical reaction, F the Faraday constant, A the geometric surface area, C_{O_2} the bulk concentration of oxygen, D_{O_2} the diffusion coefficient of oxygen in the bulk solution, ω the rotation rate in rpm, υ the kinematic viscosity of the solution, L the Nafion film thickness, C_f the reactant concentration in the Nafion film and D_f means the diffusion coefficient of oxygen in the Nafion film. Since the film thickness L was reduced to the extent that I_f became significantly larger than I_k and I_l, the influence of I_f on the measured disk current in our experiments was negligible.

Fig. 2(a) presents typical Koutecky–Levich plots for $RuFeN_x/C$ obtained at the disk potentials of 0.65 and 0.70 V(NHE). A linear relationship between I_d^{-1} and $\omega^{-1/2}$ is clearly observed and the slope remains nearly constant, regardless of the disk potential, which indicates that the electrochemical reaction follows a first-order kinetics [8]. By a linear extrapolation toward $\omega \to \infty$, I_k was calculated from Eq. (1), and the resulting values at 0.7 V(NHE) were summarized in Fig. 2(b) for various bimetallic catalysts. The I_k value increases in the order of $RuCrN_x/C$, $RuTiN_x/C$, $RuPbN_x/C$, $RuCoN_x/C$ and $RuFeN_x/C$, indicating that the non-noble alloying metal in the bimetallic catalyst has a crucial role in the catalytic activity.

3.2. Physical and electrochemical characterizations of $RuFeN_x/C$ catalyst

Fig. 3 presents the powder XRD patterns of the carbon-supported $RuFeN_x$ catalyst pyrolized at 800 °C. For comparison, the XRD pattern for the RuN_x/C catalyst is also shown in Fig. 3. A broad diffraction peak resulting from the carbon support is observed around 24.5°. The XRD pattern for RuN_x/C clearly exhibits the characteristic peaks which correspond to crystalline Ru. As indicated in Fig. 3, the diffraction peaks at 38.2°, 42.0° and 43.8° are assigned to (1 0 0), (0 0 2) and (1 0 1) planes, respectively. The three characteristic diffraction peaks from $RuFeN_x/C$ shifted toward high Bragg angles, which indicates the formation of bimetallic alloy of hexagonal-structure with smaller lattice constants [9].

The TEM micrographs of FeN_x/C and $RuFeN_x/C$ are shown in Fig. 4(a) and (b), respectively. The TEM image of FeN_x/C shows relatively large particle agglomerates with diameters of 20–40 nm, while the image for $RuFeN_x$ exhibits uniformly dispersed particles as large as 5–6 nm.

According to the composition of the precursor solution, the concentrations of Ru and Fe in the supported catalyst are expected to be ca. 13 and 7 wt.%, respectively. In order to examine whether or not the formation of binary alloy leads to an enhancement of catalytic activity toward ORR, the performances of the following catalysts were compared with that of $RuFeN_x/C$:

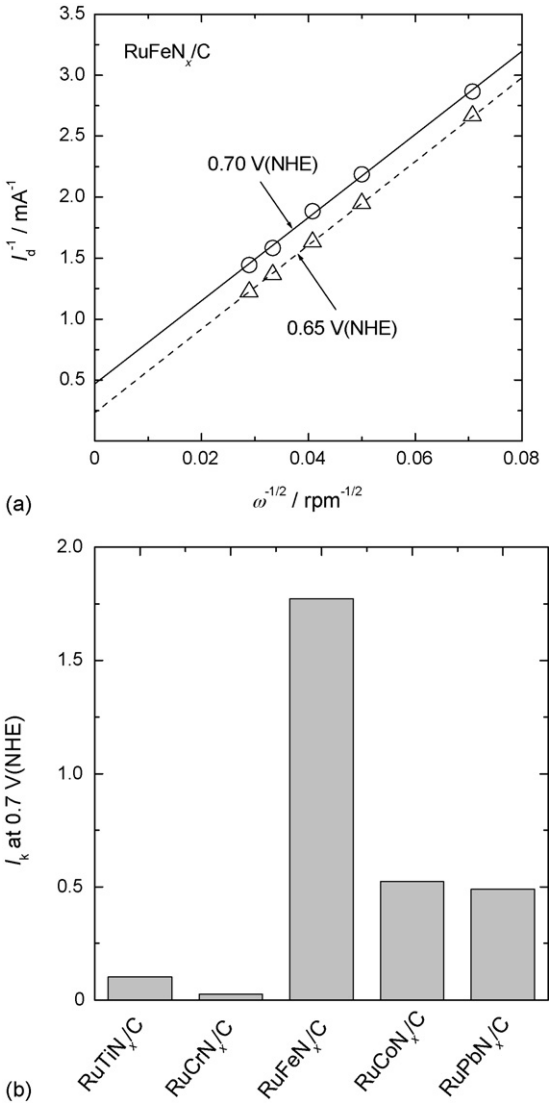

Fig. 2. (a) Koutecky–Levich plots at 0.65 and 0.70 V(NHE) measured on the $RuFeN_x/C$ catalysts, and (b) the kinetically limited currents I_k at 0.70 V(NHE) determined for various bimetallic catalysts.

(i) RuN_x/C (13 wt.% Ru) and (ii) a physical, homogeneous mixture of RuN_x/C and FeN_x/C (13 wt.% Ru and 7 wt.% Fe in the mixture) which is denoted as RuN_x/C–FeN_x/C.

Fig. 5 compares polarization curves on the ring disk electrode measured for different catalysts including the conventional Pt/C catalyst (20 wt.% Pt, E-TEK). The catalytic activity of RuN_x/C–FeN_x/C is almost similar to that of RuN_x/C due to a low activity of FeN_x/C. On the other hand, the bimetallic $RuFeN_x/C$ catalyst shows higher activity and better reduction kinetics when compared with RuN_x/C–FeN_x/C and RuN_x/C. This reflects that both Ru and Fe are responsible for the observed catalytic activity of the bimetallic alloy: namely, $RuFeN_x/C$ shows the synergetic performance which exceeds the sum of RuN_x/C and FeN_x/C's individual performances. The $RuFeN_x/C$ catalyst exhibits only 30 mV higher overpotential for ORR in comparison to the conventional Pt/C catalyst.

The percentage of H_2O_2 produced was calculated from the measured disk (I_d) and ring currents (I_r) using the following

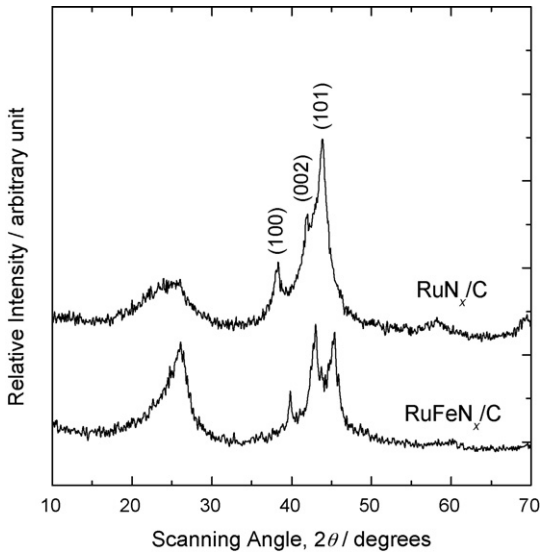

Fig. 3. XRD patterns of 20 wt.% RuN_x/C and 20 wt.% $RuFeN_x$/C.

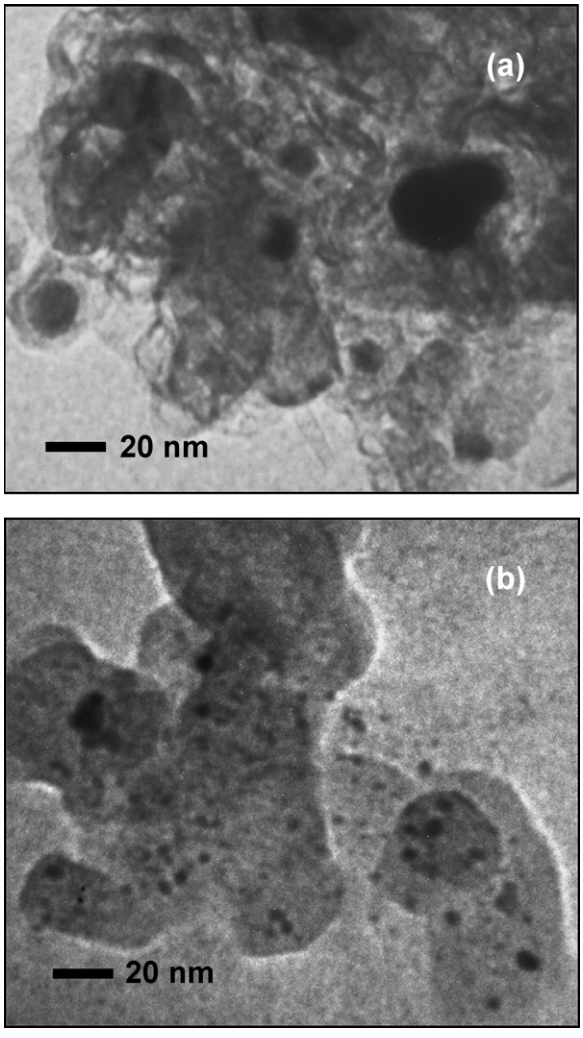

Fig. 4. TEM images of (a) 20 wt.% FeN_x/C and (b) 20 wt.% $RuFeN_x$/C.

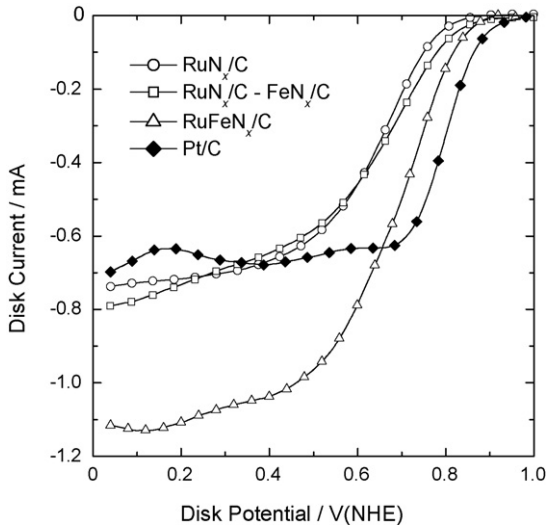

Fig. 5. Polarization curves on the rotating disk electrodes for different catalysts: RuN_x/C, RuN_x/C–FeN_x/C, $RuFeN_x$/C and Pt/C.

equation [7]:

$$\%\,H_2O_2 = \frac{200(I_r/N)}{I_d + (I_r/N)} \quad (2)$$

where N means the collection efficiency. Here, the value of N was taken as 0.39. The results are given in Table 1 as a function of disk potential for different catalysts: (i) 20 wt.% FeN_x/C, (ii) 20 wt.% $RuFeN_x$/C and (iii) 20 wt.% Pt/C. As shown in Table 1, the amount of H_2O_2 produced on FeN_x/C is even higher than 20% above 0.5 V(NHE), while alloying of Ru and Fe results in an enhanced catalytic selectivity toward the four-electron reduction of O_2 to H_2O. The bimetallic $RuFeN_x$/C catalyst generates less than 3% H_2O_2 over the whole potential range, which is slightly higher than the amount of H_2O_2 produced on the Pt/C catalyst.

Fig. 6 illustrates the performances of MEA made using the $RuFeN_x$/C cathode catalyst. The polarization curves were measured with H_2/O_2, and the open circuit potential of the MEA tested was found to be approximately 0.9 V. The initial polarization curve shows the current density of ca. 0.8 A cm^{-2} at 0.2 V and the maximum power density of ca. 0.18 W cm^{-2} at 0.55 A cm^{-2}, which are superior to the MEA performances with the Ru-based cathode catalysts reported in the literature [10,11]. From Fig. 6, it is seen that the bimetallic $RuFeN_x$/C catalyst shows no degradation of fuel cell performance even for 150 h of continuous operation, i.e. after 3500 successive cycles.

Table 1
H_2O_2 percentages determined at different disk potential for FeN_x/C, $RuFeN_x$/C and Pt/C

Disk potential (V(NHE))	% H_2O_2		
	FeN_x/C	$RuFeN_x$/C	Pt/C
0.6	31.6	2.5	0.4
0.5	22.9	2.8	0.4
0.4	19.7	2.8	0.7
0.3	16.0	2.6	1.1
0.2	12.0	2.0	1.3

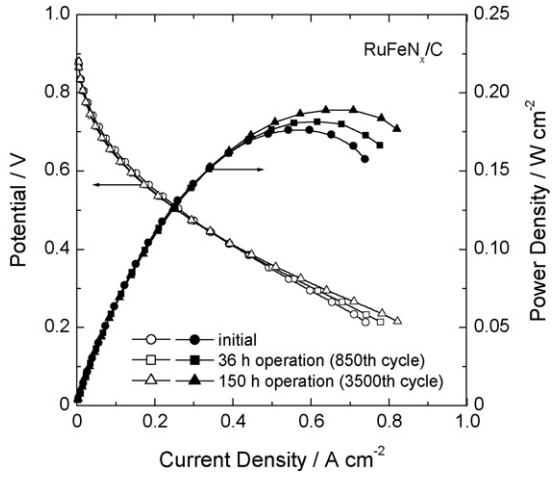

Fig. 6. Polarization curves of the MEA prepared with the $RuFeN_x$/C cathode catalyst. The experiments were performed with H_2/O_2 during successive cycling between 0.2 and 0.9 V.

4. Conclusions

Ru-based bimetallic electrocatalysts with different non-noble alloying metals were prepared on a porous carbon support using a chelation method. The catalytic activity for ORR increased in the order of $RuCrN_x$/C, $RuTiN_x$/C, $RuPbN_x$/C, $RuCoN_x$/C and $RuFeN_x$/C, indicating that the non-noble metal in the bimetallic catalyst has a crucial role in the catalytic activity. The $RuFeN_x$/C catalyst showed the onset potential for ORR as high as 0.9 V(NHE) which is comparable to that of the Pt/C catalyst. The TEM analysis indicated that the $RuFeN_x$/C catalyst consists of uniformly dispersed particles as large as 5–6 nm. The MEA prepared with the $RuFeN_x$/C cathode catalyst exhibited the maximum power density of ca. 0.18 W cm^{-2} and no performance degradation for 150 h of continuous operation.

Acknowledgement

Financial support provided by Department of Energy (DOE) is acknowledged gratefully.

References

[1] T.R. Ralph, M.P. Hogarth, Platinum Met. Rev. 46 (2002) 3–14.
[2] N. Alonso-Vante, H. Tributsch, Nature 323 (1986) 431–432.
[3] N. Alonso-Vante, M. Fieber-Erdmann, H. Rossner, E. Holub-Krappe, C. Giorgetti, A. Tadjeddine, E. Dartype, A. Fontaine, R. Frahm, J. Phys. IV France 7 (1997) 887–889.
[4] J. Maruyama, M. Inaba, Z. Ogumi, J. Electroanal. Chem. 458 (1998) 175–182.
[5] H. Tributsch, M. Bron, M. Hilgendorff, H. Schulenburg, I. Dorbandt, V. Eyert, P. Bogdanoff, S. Fiechter, J. Appl. Electrochem. 31 (2001) 739–748.
[6] L. Liu, H. Kim, J.-W. Lee, B.N. Popov, J. Electrochem. Soc., in press.
[7] U.A. Paulus, T.J. Schmidt, H.A. Gasteiger, R.J. Behm, J. Electroanal. Chem. 495 (2001) 134–145.
[8] O. Solorza-Feria, S. Ramírez-Raya, R. Rivera-Noriega, E. Ordoñez-Regil, S.M. Fernández-Valverde, Thin Solid Films 311 (1997) 164–170.
[9] H.-J. Moon, W.-D. Kim, S.-J. Oh, J. Park, J.-G. Park, E.-J. Cho, J.-I. Lee, H.-C. Ri, J. Korean Phys. Soc. 36 (2000) 49–53.
[10] R.G. González-Huerta, J.A. Chávez-Carvayar, O. Solorza-Feria, J. Power Sources 153 (2006) 11–17.
[11] K. Suárez-Alcántara, A. Rodríguez-Castellanos, R. Dante, O. Solorza-Feria, J. Power Sources 157 (2006) 114–120.